J Sci Comput (2011) 47: 216–238
DOI 10.1007/s10915-010-9435-5

Improvement of Convergence to Steady State Solutions of Euler Equations with the WENO Schemes

Shuhai Zhang · Shufen Jiang · Chi-Wang Shu

Received: 21 July 2010 / Revised: 26 October 2010 / Accepted: 29 November 2010 /
Published online: 9 December 2010

Abstract The convergence to steady state solutions of the Euler equations for high order weighted essentially non-oscillatory (WENO) finite difference schemes with the Lax-Friedrichs flux splitting (Jiang and Shu, in J. Comput. Phys. 126:202–228, 1996) is investigated. Numerical evidence in Zhang and Shu (J. Sci. Comput. 31:273–305, 2007) indicates that there exist slight post-shock oscillations when we use high order WENO schemes to solve problems containing shock waves. Even though these oscillations are small in their magnitude and do not affect the "essentially non-oscillatory" property of the WENO schemes, they are indeed responsible for the numerical residue to hang at the truncation error level of the scheme instead of settling down to machine zero. Differently from the strategy adopted in Zhang and Shu (J. Sci. Comput. 31:273–305, 2007), in which a new smoothness indicator was introduced to facilitate convergence to steady states, in this paper we study the effect of the local characteristic decomposition on steady state convergence. Numerical tests indicate that the slight post-shock oscillation has a close relationship with the local characteristic decomposition process. When this process is based on an average Jacobian at the cell interface using the Roe average, as is the standard procedure for WENO schemes, such post-shock oscillation appears. If we instead use upwind-biased interpolation to approximate the physical variables including the velocity and enthalpy on the cell interface to compute the left and right eigenvectors of the Jacobian for the local characteristic decomposition, the slight post-shock oscillation can be removed or reduced significantly and the numerical residue settles down to lower values than other WENO schemes and can

S. Zhang
State Key Laboratory of Aerodynamics, China Aerodynamics Research and Development Center, Mianyang, Sichuan 621000, China
e-mail: zhang_shuhai@tom.com

S. Jiang
Mianyang Zhengyu Science and Technology Company, Mianyang, Sichuan 621000, China

C.-W. Shu (✉)
Division of Applied Mathematics, Brown University, Providence, RI 02912, USA
e-mail: shu@dam.brown.edu

reach machine zero for many test cases. This new procedure is also effective for higher order WENO schemes and for WENO schemes with different smoothness indicators.

Keywords WENO reconstruction · WENO interpolation · Steady state solution

1 Introduction

In this paper, we continue our work in [20] to further study the convergence of high order weighted essentially nonoscillatory (WENO) finite difference schemes [8] to solve steady state solutions of the conservation law

$$\frac{\partial U}{\partial t} + \sum_{i=1}^{d} \frac{\partial F_i(U)}{\partial x_i} = 0 \tag{1.1}$$

given by the equation

$$\sum_{i=1}^{d} \frac{\partial F_i(U)}{\partial x_i} = 0. \tag{1.2}$$

We obtain the steady state solutions of (1.2) through a total variation diminishing (TVD) Runge-Kutta time marching scheme [16]. Here U is the vector of the conservative variables, $F_i(U)$ is the (usually nonlinear) flux function in the i-th direction, and d is the spatial dimension. In all the numerical tests we use the Euler equations of compressible gas dynamics as examples.

Euler equations (1.1) or (1.2) contain discontinuous solutions, which are known as shock waves or contact lines. Across these discontinuities, the physical variables, such as density, pressure and velocity, may be discontinuous. Capturing such discontinuities well is a key requirement in the design of numerical schemes. There are many choices of shock capturing schemes such as the TVD schemes [5], essentially non-oscillatory (ENO) schemes [6, 16], and WENO schemes [8, 9]. The finite difference WENO schemes [8], because of their simplicity and efficiency for multi-dimensional calculations, have been extensively used in the simulation of the multi-scale and delicate structures of physical phenomena, for example in problems related to shock turbulence interaction and shock vortex interaction [18, 19]. For a review of WENO schemes, see [15].

However, like most other high order shock capturing schemes, WENO schemes also suffer from problems during convergence to steady states. When we use WENO schemes to simulate the solution of the steady equation (1.2) by marching with the unsteady equation (1.1), the residue often stops decreasing at the truncation error level of the scheme, far above machine zero, although the flow variables do not change significantly with further iteration. In our earlier work [20], we have performed extensive numerical tests to demonstrate this difficulty. A major problem influencing steady state convergence is the existence of slight post-shock oscillations. When we use WENO schemes to solve a steady problem that contains shock waves, there usually exist slight post-shock oscillations [20]. Even though these slight post-shock oscillations do not influence the aerodynamic character, they can be confused with the multi-scale features such as the acoustic signals and turbulence fluctuation. For instance, the radiated pressure fluctuation of the "terrifyingly loud" noise of 114 dB of turbo-jets [3] is less than 10^{-4}, which might be smaller than the "slight" post-shock oscillation for a WENO simulation of a Mach 2 steady shock wave.

There are many factors which may influence the slight post-shock oscillation and slow steady state convergence. Serna and Marquina [14] designed a smooth limiter to reconstruct the flux. Although the authors did not discuss convergence to steady states for their scheme, the use of the limiter actually improves convergence to steady states [20]. Zhang and Shu [20] proposed a new smoothness indicator for the fifth order WENO scheme. With this new smoothness indicator, the slight post-shock oscillation is either removed or significantly reduced. The residue can settle down to machine zero for many one and two dimensional test cases. However, it seems difficult to generalize such smoothness indicators to higher order WENO schemes. Also, this new smoothness indicator may result in a degeneracy of accuracy at certain higher order critical points [7].

In this paper we adopt a different approach than that in [20] and concentrate on an investigation of the effect of the local characteristic decomposition procedure to steady state convergence. We perform extensive numerical tests to identify the close relationship between the slight post-shock oscillation and the local characteristic decomposition process. It is noticed that, when this process is based on an average Jacobian at the cell interface, for example using the traditional Roe average [11], such post-shock oscillations would appear. If we instead use upwind-biased interpolation procedure to approximate the physical variables including the velocity and enthalpy on the cell interface to compute the left and right eigenvectors for the local characteristic decomposition, the slight post-shock oscillation can be either removed or reduced significantly and the residue can settle down to machine zero in many test problems. This improvement is obtained without any restriction to the WENO weights, making it easier to be generalized to higher order WENO schemes or to be applied with different WENO weights (e.g. those in [7]) to enhance accuracy.

This paper is organized as follows. In the second section, we give a brief overview of the methodology of WENO schemes, including the traditional procedure to perform the local characteristic decomposition. Section 3 contains our proposed method to compute the eigenvectors during the local characteristic decomposition process. Section 4 contains numerical test and comparison results. An accuracy test is performed in Sect. 5, and concluding remarks are given in Sect. 6.

2 Methodology of WENO Schemes

In this section, we give a brief overview of the finite difference WENO schemes including the numerical fluxes, smoothness indicator, flux splitting and the discretization of the time derivative.

2.1 Numerical Fluxes of WENO Schemes

We consider the following one dimensional hyperbolic scalar equation as an example

$$u_t + f(u)_x = 0. \tag{2.1}$$

We take the positive wind direction, namely $f'(u) \geq 0$ in (2.1), as an example below. The computational domain $[x_L, x_R]$ is divided into a uniform mesh for simplicity, with a constant mesh size $\triangle x = x_{j+1} - x_j$. The conservative property of the spatial discretization is obtained by implicitly defining the numerical flux function $\hat{f}(x)$ as

$$f(u(x)) = \frac{1}{\triangle x} \int_{x-\frac{\triangle x}{2}}^{x+\frac{\triangle x}{2}} \hat{f}(\xi) d\xi. \tag{2.2}$$

Hence, the spatial derivative $f(u)_x$ at the point $x = x_i$ in (2.1) can be represented by a conservative finite difference formula

$$\frac{d\,u_i}{dt} = -\frac{1}{\triangle x}(\hat{f}_{i+\frac{1}{2}} - \hat{f}_{i-\frac{1}{2}}). \tag{2.3}$$

The right hand side will also be written in the operator form

$$L(u)_i = -\frac{1}{\triangle x}[\hat{f}_{i+\frac{1}{2}} - \hat{f}_{i-\frac{1}{2}}]. \tag{2.4}$$

The numerical flux $\hat{f}_{i+\frac{1}{2}}$ can be reconstructed by the point value $f_i = f(u_i)$ (which is the cell average of $\hat{f}(x)$, the flux function) in a r-point stencil $S^k = (x_{i-k}, x_{i-k+1}, \ldots, x_{i+s})$,

$$\hat{f}^k_{i+\frac{1}{2}} = \sum_{j=0}^{r-1} c_{kj} f_{i-k+j}, \tag{2.5}$$

where $k \geq 0$, $s \geq 0$ and $k + s + 1 = r$. This numerical flux can achieve r-th order numerical accuracy for approximating the spatial derivative $f(u)_x$

$$\frac{1}{\triangle x}(\hat{f}^k_{i+\frac{1}{2}} - \hat{f}^k_{i-\frac{1}{2}}) = f(u(x))_x|_{x=x_i} + O(\triangle x^r) \tag{2.6}$$

with suitable choices of the coefficients c_{kj}.

There are r possible candidates of such stencils and numerical fluxes $\hat{f}^k_{i+\frac{1}{2}}$, $k = 0, \ldots, r-1$. To capture the discontinuities, ENO schemes [6] are devised through "adaptive stencil", by choosing the smoothest stencil among these candidates to avoid the discontinuity. WENO schemes [8, 9] are an extension of ENO schemes. Instead of using only one stencil (the optimal stencil in some sense), a WENO scheme would use all candidate stencils through a convex combination to approximate the flux. The accuracy can be improved to the optimal order in smooth regions while the essentially non-oscillatory property near discontinuities is maintained. The WENO numerical flux is given by

$$\hat{f}^{\mathrm{WENO}}_{i+\frac{1}{2}} = \sum_{k=0}^{r-1} \omega_k \hat{f}^k_{i+\frac{1}{2}}. \tag{2.7}$$

The nonlinear weights ω_k are computed by

$$\omega_k = \frac{\alpha_k}{\alpha_0 + \alpha_1 + \cdots + \alpha_{r-1}}, \tag{2.8}$$

where

$$\alpha_k = \frac{d_k}{(\varepsilon + IS_k)^p}, \quad k = 0, 1, \ldots, r-1. \tag{2.9}$$

Here d_k are the linear weights and ε is a small positive number which is introduced to avoid the denominator becoming zero. In our later tests, we take $\varepsilon = 10^{-6}$ and the power $p = 2$. IS_k is the smoothness indicator of the flux function in the k-th substencil which is taken as

in Jiang and Shu [8] as

$$IS_k = \sum_{l=1}^{r-1} \int_{x_{i-\frac{1}{2}}}^{x_{i+\frac{1}{2}}} \triangle x^{2l-1} \left(\frac{\partial^l \hat{f}^k(x)}{\partial^l x} \right)^2 dx \tag{2.10}$$

where $\hat{f}^k(x)$ is the reconstruction polynomial based on the substencil S^k.

2.1.1 High Order WENO Schemes

In this subsection we document the fifth and seventh order finite difference WENO schemes [1, 8] that we will use later in our numerical tests.

(a) Fifth order WENO scheme ($r = 3$).

In the case of $r = 3$, the fifth order WENO scheme was obtained by Jiang and Shu [8], which has been used most often among various WENO schemes in applications. The three third order numerical fluxes from the three substencils are

$$\begin{aligned} \hat{f}^0_{j+1/2} &= \frac{1}{3} f(u_{j-2}) - \frac{7}{6} f(u_{j-1}) + \frac{11}{6} f(u_j), \\ \hat{f}^1_{j+1/2} &= -\frac{1}{6} f(u_{j-1}) + \frac{5}{6} f(u_j) + \frac{1}{3} f(u_{j+1}), \\ \hat{f}^2_{j+1/2} &= \frac{1}{3} f(u_j) + \frac{5}{6} f(u_{j+1}) - \frac{1}{6} f(u_{j+2}). \end{aligned} \tag{2.11}$$

The linear weights are given by

$$d_0 = \frac{1}{10}, \qquad d_1 = \frac{6}{10}, \qquad d_2 = \frac{3}{10}, \tag{2.12}$$

and the nonlinear weights are given by

$$\omega_r = \frac{\alpha_r}{\sum_{i=0}^{2} \alpha_i}, \qquad \alpha_r = \frac{d_r}{(\varepsilon + IS_r)^p}, \qquad r = 0, 1, 2. \tag{2.13}$$

IS_r are the smoothness indicators which are given by

$$\begin{aligned} IS_0 &= \frac{13}{12}(f_{j-2} - 2f_{j-1} + f_j)^2 + \frac{1}{4}(f_{j-2} - 4f_{j-1} + 3f_j)^2, \\ IS_1 &= \frac{13}{12}(f_{j-1} - 2f_j + f_{j+1})^2 + \frac{1}{4}(f_{j-1} - f_{j+1})^2, \\ IS_2 &= \frac{13}{12}(f_j - 2f_{j+1} + f_{j+2})^2 + \frac{1}{4}(3f_j - 4f_{j+1} + f_{j+2})^2. \end{aligned} \tag{2.14}$$

Henrich et al. [7] noticed that the nonlinear weights with the smoothness indicator (2.14) may lose accuracy at certain smooth extrema. They introduced a mapping function:

$$g_r(\omega) = \frac{\omega(d_r + (d_r)^2 - 3d_r\omega + \omega^2)}{(d_r)^2 + (1 - 2d_r)\omega}, \tag{2.15}$$

where $\omega \in [0,1]$ and $r = 0, 1, 2$. This function is monotonically increasing with a finite slope and $g_r(0) = 0$, $g_r(1) = 1$, $g_r(d_r) = d_r$, $g_r'(d_r) = 0$, and $g_r''(d_r) = 0$. The mapped weights are given by:

$$\omega_r^M = g_r(\omega_r), \tag{2.16}$$

where ω_r are computed by (2.13) and (2.14). This mapped WENO scheme can improve accuracy at smooth extrema. An additional advantage is that accuracy depends much less on the magnitude of the parameter ε and hence it can be taken close to machine zero. We refer to [7] for more details.

Borges et al. [2] defined a new smoothness indicator by

$$\beta_r^z = \frac{IS_r + \varepsilon}{IS_r + \tau_5 + \varepsilon}, \quad r = 0, 1, 2 \tag{2.17}$$

where $\tau_5 = |IS_2 - IS_0|$, and the nonlinear weights are defined by

$$\omega_r^z = \frac{\alpha_r^z}{\sum_{l=0}^{2} \alpha_l^z}, \qquad \alpha_r^z = \frac{d_r}{\beta_r^z} = d_r \left(1 + \frac{\tau_5}{\beta_r + \varepsilon}\right), \quad r = 0, 1, 2. \tag{2.18}$$

With this new smoothness indicator, the improved WENO scheme has similar accuracy at smooth extrema as the mapped WENO, while the CPU cost is reduced by about 25%, since no mapping is necessary.

(b) Seventh order WENO scheme ($r = 4$).

In the case of $r = 4$, the seventh order WENO scheme was obtained by Balsara and Shu [1]. The four fourth order numerical fluxes from the four substencils are

$$\begin{aligned}
\hat{f}^0_{i+\frac{1}{2}} &= -\frac{1}{4} f_{i-3} + \frac{13}{12} f_{i-2} - \frac{23}{12} f_{i-1} + \frac{25}{12} f_i, \\
\hat{f}^1_{i+\frac{1}{2}} &= \frac{1}{12} f_{i-2} - \frac{5}{12} f_{i-1} + \frac{13}{12} f_i + \frac{1}{4} f_{i+1}, \\
\hat{f}^2_{i+\frac{1}{2}} &= -\frac{1}{12} f_{i-1} + \frac{7}{12} f_i + \frac{7}{12} f_{i+1} - \frac{1}{12} f_{i+2}, \\
\hat{f}^3_{i+\frac{1}{2}} &= \frac{1}{4} f_i + \frac{13}{12} f_{i+1} - \frac{5}{12} f_{i+2} + \frac{1}{12} f_{i+3}.
\end{aligned} \tag{2.19}$$

The linear weights are given by

$$d_0 = \frac{1}{35}, \qquad d_1 = \frac{12}{35}, \qquad d_2 = \frac{18}{35}, \qquad d_3 = \frac{4}{35}, \tag{2.20}$$

and the smoothness indicators are

$$\begin{aligned}
IS_0 &= f_{i-3}(547f_{i-3} - 3882f_{i-2} + 4642f_{i-1} - 1854f_i) \\
&\quad + f_{i-2}(7043f_{i-2} - 17246f_{i-1} + 7042f_i) \\
&\quad + f_{i-1}(11003f_{i-1} - 9402f_i) + 2107f_i^2, \\
IS_1 &= f_{i-2}(267f_{i-2} - 1642f_{i-1} + 1602f_i - 494f_{i+1}) \\
&\quad + f_{i-1}(2843f_{i-1} - 5966f_i + 1922f_{i+1}) \\
&\quad + f_i(3443f_i - 2522f_{i+1}) + 547f_{i+1}^2, \\
IS_2 &= f_{i-1}(547f_{i-1} - 2522f_i + 1922f_{i+1} - 494f_{i+2}) \\
&\quad + f_i(3443f_i - 5966f_{i+1} + 1602f_{i+2}) \\
&\quad + f_{i+1}(2843f_{i+1} - 1642f_{i+2}) + 267f_{i+2}^2, \\
IS_3 &= f_i(2107f_i - 9402f_{i+1} + 7042f_{i+2} - 1854f_{i+3}) \\
&\quad + f_{i+1}(11003f_{i+1} - 17246f_{i+2} + 4642f_{i+3}) \\
&\quad + f_{i+2}(7043f_{i+2} - 3882f_{i+3}) + 547f_{i+3}^2.
\end{aligned} \tag{2.21}$$

2.2 Local Characteristic Decomposition for Conservative Law Systems

For system of equations, such as the Euler equations (1.2), the WENO reconstruction is usually implemented in the local characteristic fields, to more effectively avoid spurious oscillations. Let $A_{i+\frac{1}{2}}$ denote the Jacobian $\frac{\partial F}{\partial U}$ at the cell interface $x_{i+\frac{1}{2}}$. The left and right eigenvectors of $A_{i+\frac{1}{2}}$ are denoted by L_s and R_s, for $s = 1, 2, \ldots, m$. Then, the scalar WENO reconstruction procedure can be applied to each of the characteristic fields

$$\hat{F}^k_{i+\frac{1}{2},s} = \sum_{j=0}^{r-1} c_{kj} L_s F_{i-k+j}, \tag{2.22}$$

$$\hat{F}^{\mathrm{WENO}}_{i+\frac{1}{2},s} = \sum_{k=0}^{r-1} \omega_{k,s} \hat{F}^k_{i+\frac{1}{2},s}. \tag{2.23}$$

The nonlinear weights $\omega_{k,s}$ are computed in the local characteristic fields

$$\omega_{k,s} = \omega_k(L_s F_{i+k-r+1}, \ldots, L_s F_{i+k}). \tag{2.24}$$

When the WENO reconstruction is finished in each characteristic field, the numerical fluxes that are obtained in each characteristic field can be projected back to the component space by

$$\hat{F}^{\mathrm{WENO}}_{i+\frac{1}{2}} = \sum_{s=1}^{m} \hat{F}^{\mathrm{WENO}}_{i+\frac{1}{2},s} R_s. \tag{2.25}$$

Traditionally, the left and right eigenvectors L_s and R_s are computed from the physical variables including velocity and enthalpy on the cell interface $x_{i+\frac{1}{2}}$ that are often taken as

the Roe average [11] from the physical values at the two neighboring points x_i and x_{i+1}. The Roe average is defined through the mean value theorem

$$F(U_{i+1}) - F(U_i) = A(U_{i+\frac{1}{2}})(U_{i+1} - U_i).$$

For the Euler equations, let ρ be the density, the other physical variables for the Roe average can be obtained by

$$U_{i+\frac{1}{2}} = \frac{\sqrt{\rho}_i}{\sqrt{\rho}_i + \sqrt{\rho}_{i+1}} U_i + \frac{\sqrt{\rho}_{i+1}}{\sqrt{\rho}_i + \sqrt{\rho}_{i+1}} U_{i+1}, \tag{2.26}$$

and then the left and right eigenvectors L_s and R_s of the Jacobian matrix $A_{i+\frac{1}{2}}$ can be computed by

$$L_s = L_s(U_{i+\frac{1}{2}}), \qquad R_s = R_s(U_{i+\frac{1}{2}}). \tag{2.27}$$

If the Roe average is not readily available, the simple arithmetic mean

$$U_{i+\frac{1}{2}} = \frac{1}{2}(U_i + U_{i+1}) \tag{2.28}$$

is also often used in the computation of left and right eigenvectors L_s and R_s.

2.3 Flux Splitting

The purpose of flux splitting is to introduce the correct upwinding. In general, the flux can be split into two parts:

$$f(u) = f^+(u) + f^-(u), \tag{2.29}$$

where $\frac{df^+(u)}{du} \geq 0$ and $\frac{df^-(u)}{du} \leq 0$. For the system case, this means that the eigenvalues of $\frac{df^+(u)}{du}$ are all non-negative, and those of $\frac{df^-(u)}{du}$ are all non-positive. The simplest and commonly used flux splitting is the Lax-Friedrichs flux splitting

$$f^\pm(u) = \frac{1}{2}(f(u) \pm \alpha u), \tag{2.30}$$

where $\alpha = \max |f'(u)|$ with the maximum taken over some relevant range of u.

2.4 Time Discretization

After the spatial derivative is discretized with the WENO scheme, we obtain a set of ordinary differential equations (ODEs):

$$\frac{du}{dt} = L(u). \tag{2.31}$$

The operator $L(u)$ is represented in (2.4). This set of ODEs can be discretized by an ODE solver, for example the third order TVD Runge-Kutta method [16] as follows:

$$\begin{aligned} u^{(1)} &= u^n + \triangle t L(u^n), \\ u^{(2)} &= \frac{3}{4}u^n + \frac{1}{4}u^{(1)} + \frac{1}{4}\triangle t L(u^{(1)}), \\ u^{n+1} &= \frac{1}{3}u^n + \frac{2}{3}u^{(2)} + \frac{2}{3}\triangle t L(u^{(2)}). \end{aligned} \tag{2.32}$$

3 Improvement of Convergence to Steady States

Like many high order accurate shock capturing schemes, WENO schemes also suffer from difficulties in their convergence toward steady state solutions, as demonstrated extensively in [20]. In [20], we proposed a new smoothness indicator, differently from (2.10), for the fifth order WENO scheme. With this new smoothness indicator, the residue of the fifth order WENO scheme for typical steady states can settle down to machine zero. However, for certain types of critical points (zeros of certain derivatives of a smooth solution), this WENO procedure might lose accuracy, as can be verified by a Taylor expansion. It also seems difficult to generalize this new smoothness indicator to higher order WENO schemes.

Based on our numerical tests, we observe that the Roe averaging procedure in (2.26) to compute the physical variables on the cell interface for the computation of the left and right eigenvectors L_s and R_s of the Jacobian matrix $A_{i+\frac{1}{2}}$ can influence the convergence history of WENO schemes. Inspired by the approach in [4], we use upwind-biased interpolation to compute the physical variables $U_{i+\frac{1}{2}}$ on the cell interface instead of the Roe average. Upwind-biased interpolation uses only or mainly information from one side of the shock for the grid point near the shock, while the Roe average uses information equally from both sides. Intuitively, the former would be less prone to disturbance and oscillations than the latter in steady state calculations. In the upwind-biased interpolation, we choose the physical variable on the cell interface $U_{i+\frac{1}{2}} = U^{(1)}$ when $u_{i+\frac{1}{2}} \geq 0$ (here u denotes the velocity in the Euler equations) and $U_{i+\frac{1}{2}} = U^{(2)}$ when $u_{i+\frac{1}{2}} < 0$, where $U^{(1)}$ and $U^{(2)}$ are the interpolated values on the cell interface, which are computed by the first order or the second order one-sided interpolation, or the higher order upwind-biased WENO interpolation (e.g. the fifth order WENO interpolation for the fifth order WENO scheme and the seventh order WENO interpolation for the seventh order WENO scheme). We emphasize that the order of accuracy of the final WENO scheme does *not* depend on the order of interpolation here, therefore we can use, e.g. the first order interpolation here and still obtain high order accuracy for the final WENO scheme. The detailed formulae are listed below.

The first order:

$$\begin{aligned} U^{(1)} &= U_i, \\ U^{(2)} &= U_{i+1}. \end{aligned} \tag{3.1}$$

The second order:

$$\begin{aligned} U^{(1)} &= (3U_i - U_{i-1})/2, \\ U^{(2)} &= (3U_{i+1} - U_{i+2})/2. \end{aligned} \tag{3.2}$$

We could also use upwind-biased WENO interpolation procedure. The WENO interpolation procedure [10, 13] is similar to that of WENO reconstruction outlined in Sect. 2.1. Using the same stencil $S^r = (x_{i-r}, x_{i-r+1}, \ldots, x_{i+s})$ as in the WENO reconstruction procedure, the physical variable at the cell interface $U_{i+1/2}$ is interpolated. For example,

$$\hat{U}^{\mathrm{WENO}I}_{i+\frac{1}{2}} = \sum_{k=0}^{r-1} \omega_k \hat{U}^k_{i+\frac{1}{2}} \tag{3.3}$$

where $\hat{U}^k_{i+\frac{1}{2}}$ is the lower order interpolation on each substencil given by

$$\hat{U}^k_{i+\frac{1}{2}} = \sum_{j=0}^{r-1} c_{kj} U_{i-k+j}. \tag{3.4}$$

In the following, we list the WENO interpolation procedure for $U^{(1)}$ on the left-biased stencil. The formulae to interpolate $U^{(2)}$ is similar which is interpolated on the right-biased stencil.

(a) The fifth order weighted interpolation ($r = 3$).
In the case of $r = 3$, the linear fifth order interpolation is given by

$$U_{i+\frac{1}{2}} = \frac{1}{128}(3U_{i-2} - 20U_{i-1} + 90U_i + 60U_{i+1} - 5U_{i+2}). \tag{3.5}$$

The three third order interpolations from the three substencils are

$$\begin{aligned} U^0_{i+\frac{1}{2}} &= \frac{1}{8}(3U_{i-2} - 10U_{i-1} + 15U_i), \\ U^1_{i+\frac{1}{2}} &= \frac{1}{8}(-U_{i-1} + 6U_i + 3U_{i+1}), \\ U^2_{i+\frac{1}{2}} &= \frac{1}{8}(3U_i + 6U_{i+1} - U_{i+2}). \end{aligned}$$

The linear weights are given by

$$c_0 = \frac{1}{16}, \qquad c_1 = \frac{10}{16}, \qquad c_2 = \frac{5}{16}, \tag{3.6}$$

and the smoothness indicators are

$$\begin{aligned} IS_0 &= \frac{1}{4}(U_{i-2} - 4U_{i-1} + 3U_i)^2 + \frac{13}{12}(U_{i-2} - 2U_{i-1} + U_i)^2, \\ IS_1 &= \frac{1}{4}(U_{i-1} - U_{i+1})^2 + \frac{13}{12}(U_{i-1} - 2U_i + U_{i+1})^2, \\ IS_2 &= \frac{1}{4}(3U_i - 4U_{i+1} + U_{i+2})^2 + \frac{13}{12}(U_i - 2U_{i+1} + U_{i+2})^2. \end{aligned}$$

(b) The seventh order weighted interpolation ($r = 4$).
In the case of $r = 4$, the linear seventh order interpolation is given by

$$U_{i+\frac{1}{2}} = \frac{1}{1024}(-5U_{i-3} + 42U_{i-2} - 175U_{i-1} + 700U_i + 525U_{i+1} - 70U_{i+2} + 7U_{i+3}). \tag{3.7}$$

The four fourth order interpolations from the four substencils are

$$\begin{aligned} U^0_{i+\frac{1}{2}} &= \frac{1}{48}(-15U_{i-3} + 63U_{i-2} - 105U_{i-1} + 105U_i), \\ U^1_{i+\frac{1}{2}} &= \frac{1}{48}(3U_{i-2} - 15U_{i-1} + 45U_i + 15U_{i+1}), \\ U^2_{i+\frac{1}{2}} &= \frac{1}{48}(-3U_{i-1} + 27U_i + 27U_{i+1} - 3U_{i+2}), \\ U^3_{i+\frac{1}{2}} &= \frac{1}{48}(15U_i + 45U_{i+1} - 15U_{i+2} + 3U_{i+3}). \end{aligned}$$

The linear weights are given by

$$c_0 = \frac{1}{64}, \qquad c_1 = \frac{21}{64}, \qquad c_2 = \frac{35}{64}, \qquad c_3 = \frac{7}{64}, \tag{3.8}$$

and the smoothness indicators are

$$\begin{aligned} IS_0 &= U_{i-3}(79788U_{i-3} - 566568U_{i-2} + 680328U_{i-1} - 273336U_i) \\ &\quad + U_{i-2}(1027692U_{i-2} - 2523384U_{i-1} + 1034568U_i) \\ &\quad + U_{i-1}(1610892U_{i-1} - 1378728U_i) + 308748U_i^2, \end{aligned}$$

$$\begin{aligned} IS_1 &= U_{i-2}(38028U_{i-2} - 232488U_{i-1} + 228168U_i - 71736U_{i+1}) \\ &\quad + U_{i-1}(401292U_{i-1} - 847224U_i + 277128U_{i+1}) \\ &\quad + U_i(492012U_i - 364968U_{i+1}) + 79788U_{i+1}^2, \end{aligned}$$

$$\begin{aligned} IS_2 &= U_{i-1}(79788U_{i-1} - 364968U_i + 277128U_{i+1} - 71736U_{i+2}) \\ &\quad + U_i(492012U_i - 847224U_{i+1} + 228168U_{i+2}) \\ &\quad + U_{i+1}(401292U_{i+1} - 232488U_{i+2}) + 38028U_{i+2}^2, \end{aligned}$$

$$\begin{aligned} IS_3 &= U_i(308748U_i - 1378728U_{i+1} + 1034568U_{i+2} - 273336U_{i+3}) \\ &\quad + U_{i+1}(1610892U_{i+1} - 2523384U_{i+2} + 680328U_{i+3}) \\ &\quad + U_{i+2}(1027692U_{i+2} - 566568U_{i+3}) + 79788U_{i+3}^2. \end{aligned}$$

This new local characteristic decomposition procedure can be applied to different variants of WENO schemes, such as the one using the smoothness indicator proposed in [20], the one using the mapped technique proposed in [7] and the improved WENO scheme in [2].

In following, we denote the original WENO scheme given by Jiang and Shu [8] as WENO, the mapped WENO scheme in [7] as MWENO, the improved WENO scheme in [2] as ZWENO, the WENO scheme in [20] as ZSWENO. The corresponding WENO schemes using upwind-biased interpolations are denoted by U1WENO, U1MWENO, U1ZWENO and U1ZSWENO for the first order interpolation, U2WENO, U2MWENO, U2ZWENO and U2ZSWENO for the second order interpolation and UWWENO, UWMWENO, UWZWENO and UWZSWENO for the full order WENO interpolation.

4 Numerical Tests

4.1 One Dimensional Steady Shock

Our first example is a one dimensional stationary shock of the Euler equations

$$U_t + F(U)_x = 0, \tag{4.1}$$

where $U = (\rho, \rho u, e)^T$, $F(U) = (\rho u, \rho u^2 + p, u(e + p))^T$. Here ρ is the density, u is the velocity, e is the total energy, p is the pressure which is related to the total energy by $e = \frac{p}{\gamma - 1} + \frac{1}{2}\rho u^2$, the ratio of specific heat $\gamma = 1.4$.

The computational domain is $x \in [-1, 1]$. It is divided into 400 uniformly spaced mesh points. The initial condition of the flow Mach number on the left of the shock is $M_\infty = 2$. The shock is located at $x = 0$. The initial condition is given by the Rankine-Hugoniot relation [12] as follows:

$$U(x, 0) = \begin{cases} U_l & \text{if } x < 0, \\ U_r & \text{if } x \geq 0, \end{cases} \tag{4.2}$$

where

$$\begin{pmatrix} \rho_l \\ \rho_l \\ u_l \end{pmatrix} = \begin{pmatrix} \frac{1}{\gamma {M_\infty}^2} \\ 1 \\ 1 \end{pmatrix}, \qquad \begin{pmatrix} p_r \\ \rho_r \\ u_r \end{pmatrix} = \begin{pmatrix} p_l \frac{2\gamma {M_\infty}^2 - (\gamma - 1)}{\gamma + 1} \\ \frac{\frac{\gamma+1}{\gamma-1}\frac{\rho_r}{\rho_l} + 1}{\frac{\gamma+1}{\gamma-1} + \frac{\rho_r}{\rho_l}} \\ \sqrt{\gamma \frac{(2 + (\gamma - 1){M_\infty}^2)p_r}{(2\gamma {M_\infty}^2 + (1 - \gamma))\rho_r}} \end{pmatrix}.$$

The initial condition is also the exact solution of the steady one dimensional Euler equations. Hence, the solution should keep the same shape for $t \geq 0$. However, because of the Lax-Friedrichs flux splitting, the initial condition is *not* a solution of the numerical scheme. The numerical shock will be smeared across a few grid points. Figure 1 (left) is the numerical density distribution along the computational domain obtained by the fifth order WENO schemes. We can see that the result is essentially non-oscillatory: no noticeable oscillations can be observed. The numerical shock profile is quite sharp and appears monotone to the eye. Even though we can not distinguish the numerical results obtained by different WENO schemes on the global view (left figure), a significant difference can be observed from the zoomed (right) figure. It is clear that the numerical result obtained by the WENO and MWENO contains a post-shock oscillation. This post-shock oscillation is reduced significantly in the result obtained by ZWENO. However, there is a higher overshoot after the

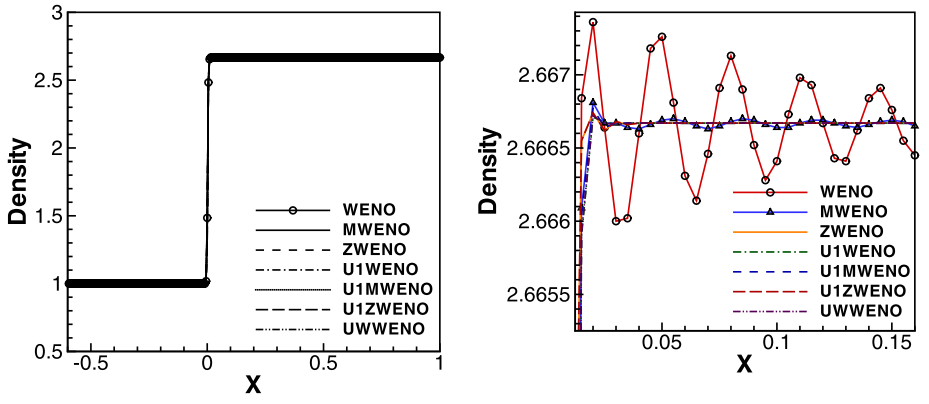

(a) Global (b) Zoomed

Fig. 1 Density distribution around the one dimensional steady shock of $M_\infty = 2$ by the fifth order WENO schemes

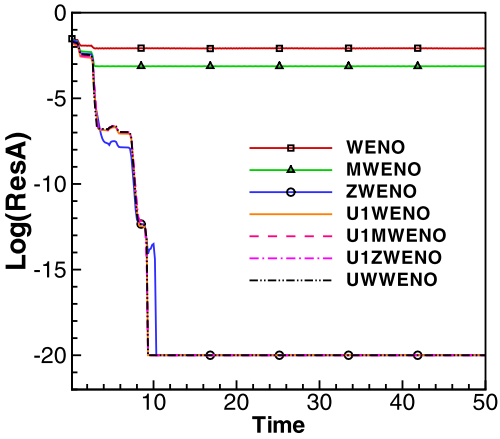

Fig. 2 The evolution of the average residue of the one dimensional steady shock of $M_\infty = 2$ by the fifth order WENO schemes

shock wave. The post-shock oscillation is removed completely with the smoothness indicator proposed by Zhang and Shu in [20] (ZSWENO) and the new technique proposed in this paper for the cases with the first order, the second order or WENO upwind-biased interpolation. Figure 2 shows the evolution of the average residue for the various fifth order WENO schemes. The average residue is defined as:

$$Res_A = \sum_{i=1}^{n} \frac{|R_i|}{N}, \tag{4.3}$$

where R_i is the local residue defined as

$$R_i = \frac{\partial \rho_i}{\partial t} = \frac{\rho_i^{n+1} - \rho_i^n}{\triangle t}, \tag{4.4}$$

and N is the total number of grid points. From Fig. 2, we observe that the average residue obtained by WENO and MWENO schemes could not converge to machine zero but hangs at a high level, around $10^{-2.2}$ for WENO and $10^{-2.9}$ for MWENO. Even though the flow variables change very little after a short time, the non-decreasing of the average residue after it reaches around $10^{-2.2}$ or $10^{-2.9}$ is a concern to many practitioners. One reason is that the residue is often used as a criterion in the computation of steady state problems to determine whether the computation should stop. If the residue could not settle down to a lower level, one can no longer use the size of the average residue to determine when to stop the computation, and must rely on experience including a visual comparison of the flow variables after many time steps to make this determination. Moreover, the post-shock oscillation is a concern in the simulation of multi-scale problems such as compressible turbulence and aeroacoustics. Among the three original WENO schemes (WENO, MWENO and ZWENO), ZWENO can settle down to machine zero for this problem. However, there is a higher overshoot after the shock wave. Using the new technique proposed in this paper, the average residue can settle down to machine zero. The residue obtained by MWENO in [7] and ZWENO [2], which can improve the accuracy near high order critical points, can also settle down to machine zero with either the smoothness indicator in [20] or the new technique proposed in this paper.

There are four kinds of previous WENO schemes, including WENO, MWENO, ZWENO and ZSWENO. Also, there are three kinds of interpolations for the physical variable in the

Table 1 The (base 10) logarithm of the residue for the one dimensional steady shock of $M_\infty = 2$ by the fifth order WENO schemes with different convergence improvement techniques

The accuracy order of the interpolation	WENO	MWENO	ZWENO	ZSWENO
First	−20	−20	−20	−20
Second	−20	−20	−20	−20
WENO5	−20	−20	−20	−20

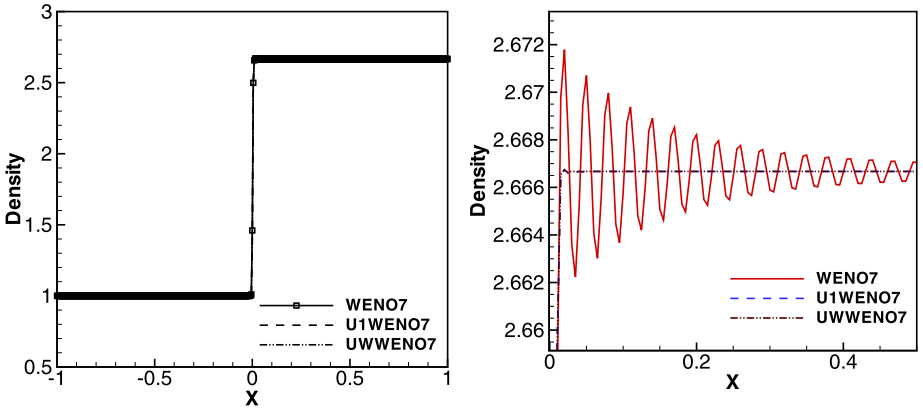

(a) Global (b) Zoomed

Fig. 3 Density distribution around the one dimensional steady shock of $M_\infty = 2$ by the seventh order WENO schemes

cell interface, namely the first order interpolation, the second order interpolation and the full order WENO interpolation. If we plot all numerical results in one figure, we could not distinguish them from each other. Hence, we just list the residue magnitudes by different schemes in Table 1. It is clear that the residues of all WENO schemes combined with the new technique can settle down to machine zero.

Figure 3 contains the density distribution obtained by the seventh order WENO schemes. From the zoomed figure shown in Fig. 3(b), we can observe that there is an even stronger post-shock oscillation for the regular seventh order WENO scheme (WENO7) compared with the fifth order version. Fortunately, this post-shock oscillation is again completely removed by the new technique in this paper (U1WENO7, UWWENO7). Figure 4 shows the average residue of the seventh order WENO schemes. Again, the average residue from the original WENO scheme hangs at a high level of $10^{-1.5}$. Using our new technique, it goes approximately to machine zero.

4.2 135° and 120° Oblique Steady Shock Waves

Our second test case is a 135° oblique steady shock wave which is also tested for the smoothness indicator in [20]. The flow Mach number on the left of the shock is $M_\infty = 2$. The computational domain is $0 \le x \le 4$ and $0 \le y \le 2$. The initial oblique shock passes through the point $(3, 0)$. The domain is divided into 200×100 equally spaced points with $\triangle x = \triangle y$. Instead of using a periodic boundary condition along the shock wave as in [20], we use the theoretical shock solution in the ghost points that are defined by the Rankine-Hugoniot

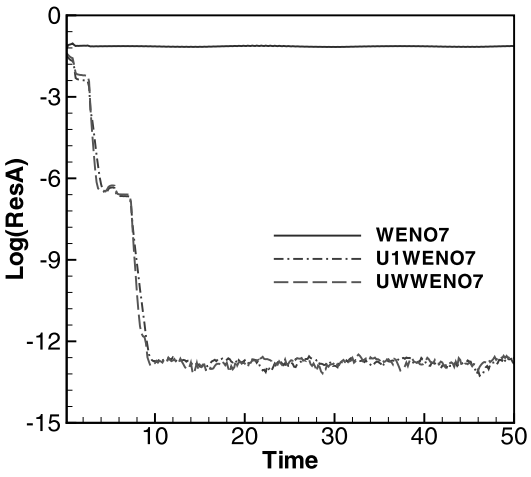

Fig. 4 The evolution of the average residue of the one dimensional steady shock of $M_\infty = 2$ by the seventh order WENO schemes

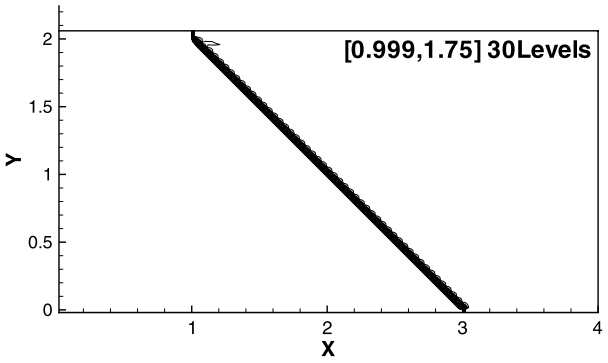

Fig. 5 Density contours for a 135° oblique shock wave obtained from the fifth order original WENO scheme

relation [12]. Figure 5 contains the density contours obtained by the original fifth order WENO scheme. Figure 6 contains the zoomed density distribution along the horizontal line of $y = 1$ and the evolution of the average residues of different types of WENO schemes. From the zoomed density distribution, we can observe that WENO suffers from a rather strong post-shock oscillation similar to the 1D case. ZWENO and U1ZWENO have the strongest overshoot after the shock wave, although the post-shock oscillation is reduced significantly. With the smoothness indicator proposed in [20], there is still an overshoot after the shock wave. U1WENO, U1MWENO and UWWENO offer the best results. There is no overshoot, and the post-shock oscillation basically disappears. The residue goes approximately to machine zero. We remark that there is a strong influence of boundary condition treatments to steady state convergence. With the periodic boundary condition, the residue of ZSWENO can go to machine zero [20]. However, with the boundary condition in this paper, the residue of ZSWENO still hangs at a rather high level of $10^{-4.4}$. The WENO scheme with the new technique of this paper can settle down to 10^{-12}, which is approximately machine zero. In Table 2 we list the residue of different schemes. It is clear that the first order upwind interpolation can offer the best convergence result among all schemes.

We next test another example which is a 120° oblique steady shock wave. The flow condition is the same as above except for the angle of the shock wave. In this case, lines parallel to the shock no longer land on grid points. Hence, we compute the problem in a

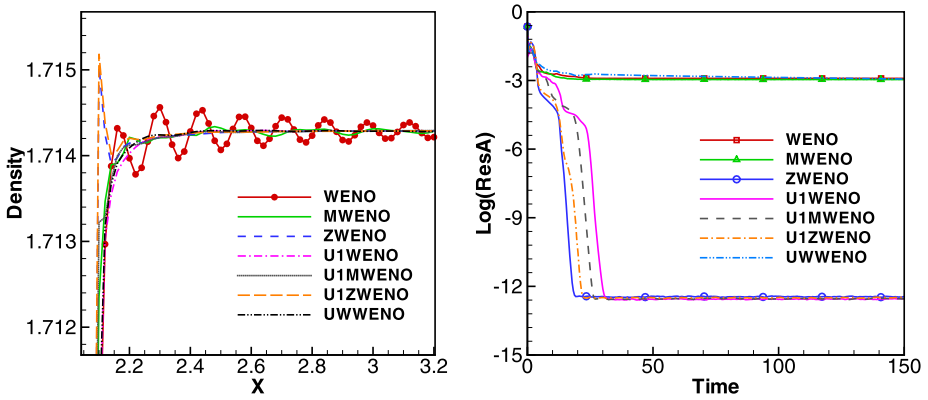

Fig. 6 Zoomed density distribution (*left*) and the evolution of the average residue (*right*) for a 135° oblique steady shock of $M_\infty = 2$ by the fifth order WENO schemes

Table 2 The (base 10) logarithm of the residue for the 135° oblique shock wave by the fifth order WENO schemes

The accuracy order of the interpolation	WENO	MWENO	ZWENO	ZSWENO
First	−12.5	−12.5	−12.5	−4.5
Second	−11.9	−12.3	−2.7	−3.4
WENO5	−3.2	−4.9	−12.5	−3.7
Roe average	−2.9	−3.0	−12.5	−4.4

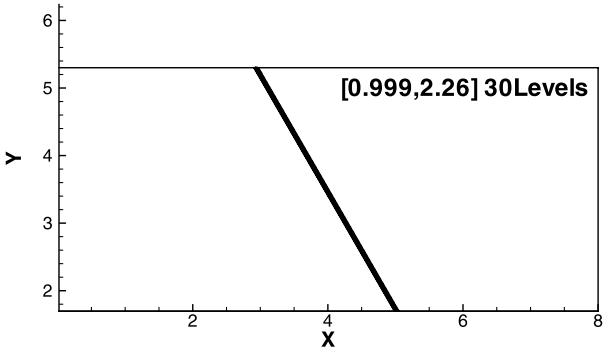

Fig. 7 Density contours for a 120° oblique shock wave obtained from the fifth order WENO scheme

larger computational domain, and use the result as an initial condition for our computation in a smaller computational domain. In this computation, the physical values in the ghost points are taken to be those obtained from the computation in the larger domain. Figure 7 contains the density contours obtained by the original fifth order WENO scheme. Figure 8 contains the zoomed density distribution along the horizontal line $y = 3.5$ and the evolution of the average residue. From the zoomed density distribution, we observe that there are significant post-shock oscillations obtained from all WENO schemes. Again, ZWENO has the strongest overshoot after the shock wave, which is reduced significantly by the use of the new technique of this paper. The average residue obtained by this new technique is also

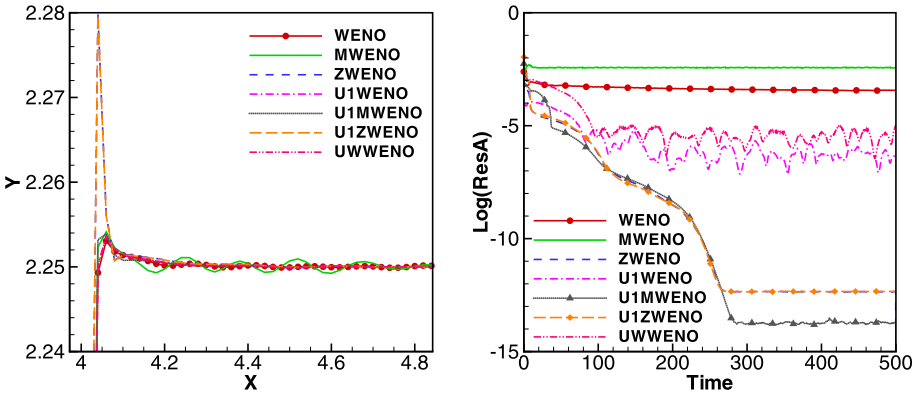

Fig. 8 Zoomed density distribution (*left*) and the evolution of the averaged residue (*right*) for a 120° oblique steady shock of $M_\infty = 2$ by the fifth order WENO schemes

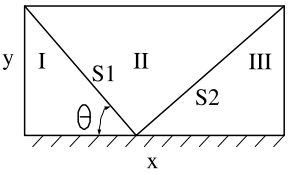

Fig. 9 Schematic diagram of the regular shock reflection

much lower than the original ones. For this (more difficult) test case, the residue goes close to machine zero only for the U1ZWENO and U1MWENO cases.

4.3 Regular Shock Reflection

The regular shock reflection is a typical two dimensional steady flow which is also tested for the smoothness indicator in [20]. The flow structure is schematically shown in Fig. 9. The impinging shock S_1 and the reflected shock S_2 separate the domain into three parts I, II and III. The corresponding physical variables are U_1, U_2 and U_3 respectively. They can be computed by the Rankine-Hugoniot relationship [12]. In our case, the flow Mach number in region I is 2.9. The impinging angle is $\theta = 29°$. More details can be found in [20].

In this example, there are additional difficulties that can hinder the steady state convergence. There are multiple shock waves which cross the boundary including at the corners of the domain. Also, the angles between the impinging shock wave with the x-axis and the reflected shock wave with the x-axis are different. Hence, the lines parallel to the shock waves cannot all land on the grid points. We have not found a completely satisfactory boundary treatment for this example. As a result, the new technique proposed in this paper does not work as well compared with the previous examples.

Figure 10 contains the density contours for the numerical results obtained by the fifth order WENO, ZSWENO, U1WENO and U1ZSWENO schemes. We can observe the numerical results by both WENO and U1WENO have obvious post-shock oscillations, which are reduced significantly by ZSWENO and U1ZSWENO. This kind of post-shock oscillations can be observed more clearly in the distribution of the density along the line of $y = 0.5$, which is shown in the left figure of Fig. 11. Due to the reduction of the post-shock oscillations, the convergence behavior of ZSWENO and U1ZSWENO is better than others,

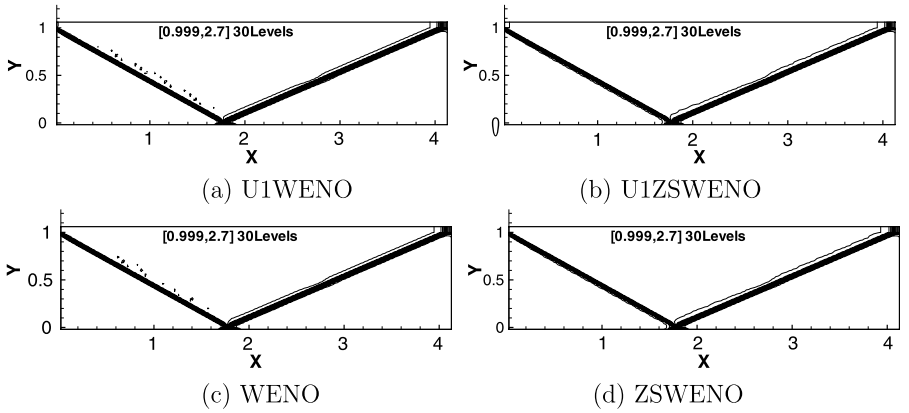

Fig. 10 Density contours for the regular shock reflection with $M_\infty = 2.9$, $\theta = 29°$ by the fifth order WENO schemes

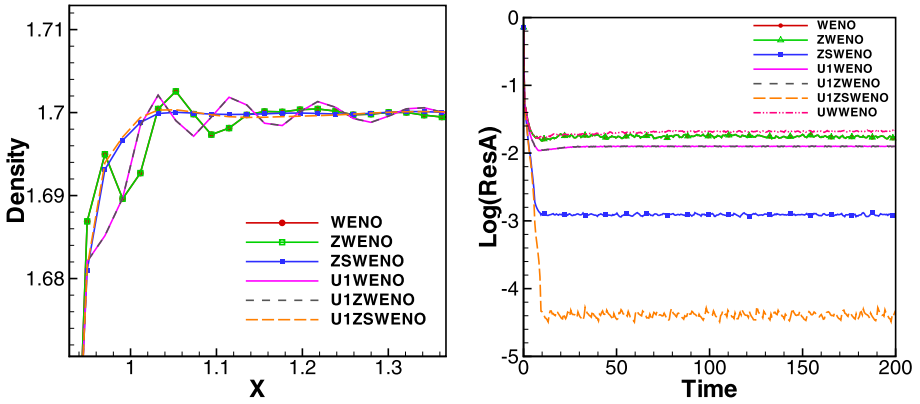

Fig. 11 Regular shock reflection with $M_\infty = 2.9$, $\theta = 29°$ by the fifth order WENO schemes. *Left*: zoomed density distribution near the impinging shock $S1$ along the line $y = 0.5$. *Right*: the evolution of the average residue

Table 3 The (base 10) logarithm of the residue for the regular shock reflection by the fifth order WENO schemes

The accuracy order of the interpolation	WENO	ZWENO	ZSWENO
First	−1.90	−1.90	−4.40
Second	−1.70	−1.70	−2.92
WENO5	−1.69	−1.69	−2.96
Roe average	−1.75	−1.75	−2.93

as shown in the right figure of Fig. 11. Other methods, including U1WENO, U1ZWENO and UWWENO, have similar behavior as the original WENO scheme. In Table 3, we list the residue by different schemes. We can observe that our new technique can improve the convergence behavior but cannot achieve close to machine zero residue for this example.

Based on our numerical tests on residue convergence, it can be observed that the WENO schemes combined with the first order or the WENO upwind-biased interpolation have the best convergence performance for steady state computation. The first order interpolation has the same CPU cost as the original WENO scheme based on the Roe average, while the CPU cost of the WENO upwind-biased interpolation is almost double that of the original WENO scheme.

5 Accuracy test

In this section, we test the accuracy of the WENO schemes. In the first example, we have adjusted the time step to $\Delta t = \Delta x^{\frac{5}{3}}$ for the 5th order WENO scheme so that the time discretization error will not dominate.

Because the technique that involves changing the Roe average to upwind-biased interpolation in the local characteristic decomposition process is relevant only for systems, our example to test the accuracy of the scheme is for the two dimensional unsteady Navier-Stokes equations. The Navier-Stokes equations with source terms are given by

$$U_t + F(U)_x + G(U)_y = F_v(U, \nabla U)_x + G_v(U, \nabla U)_y + S, \tag{5.1}$$

where the exact forms of the inviscid fluxes $F(U)$ and $G(U)$, and the viscous fluxes $F_v(U, \nabla U)$ and $G_v(U, \nabla U)$ can be found in, e.g. [18]. The computational domain is $0 \leq x \leq 2\pi$ and $0 \leq y \leq 2\pi$. The test functions are given by: $\rho = 1$, $u = 1 + \frac{1}{10}\sin(x + y + t)$, $v = 1 - \frac{1}{10}\sin(x + y + t)$, $p = \frac{1}{\gamma M_\infty^2}$, $e = \frac{p}{\gamma - 1} + \frac{1}{2}\rho(u^2 + v^2)$, $M_\infty = 0.3$, and $\gamma = 1.4$. It is the "exact solution" of (5.1) with the source term $S = U_t^{tf} + F(U^{tf})_x + G(U^{tf})_y - F_v(U^{tf}, \nabla U^{tf})_x - G_v(U^{tf}, \nabla U^{tf})_y$, where the superscript tf represents the test function listed above. The viscous terms $F_v(U, \nabla U)_x$ and $G_v(U, \nabla U)_y$ are discretized by central difference formulae of comparable orders of accuracy. We refer to [18] for more details of this test case.

In Table 4 we list the L_1 and L_∞ errors and numerical orders of accuracy at $t = 1$ for the energy. We observe that all WENO schemes can achieve fifth order accuracy very quickly. The magnitude of errors is almost the same for the various WENO schemes and different characteristic decomposition Jacobians.

To further test the performance near smooth extrema of the WENO schemes, we compute the shock density wave interaction problem in [17]. It describes the interaction of a Mach 3 shock with a density wave. A Mach 3 shock is initially located at $x = -4$ and moves toward the right. A sine wave is superposed to the density in the right region to the shock which is given by $(\rho, u, p) = (1 + a\sin(5x), 0, 1)$. The amplitude of the sine wave is $a = 0.2$. The value downstream of the shock wave is computed by the Rankine-Hugoniot relation [12].

Figure 12 shows the density distribution of the numerical solutions of various fifth order WENO schemes. Even though the procedure of the characteristic projection does not affect the order of accuracy of the WENO scheme, the numerical result obtained by the first order interpolation (U1WENO) is slightly worse than the original WENO scheme (WENO) near the extrema. It is however slightly better than ZSWENO. On the other hand, the WENO interpolation (UWWENO) is the same as the original WENO scheme.

Figures 13 shows the density distribution of the numerical solutions of various seventh order WENO schemes. We again observe that the WENO interpolation (UWWENO7) is the same as the original WENO scheme (WENO7). Both of them are slightly better than the result by the first order interpolation (U1WENO7).

Table 4 L_1 and L_∞ errors and numerical orders of accuracy for the energy on the two dimensional Navier-Stokes equations. N is the number of grid points per dimension in a uniform mesh. $t = 1$

Method	N	L_1 error	L_1 order	L_∞ error	L_∞ order
WENO	20	$6.97e{-5}$		$1.62e{-4}$	
	40	$2.54e{-6}$	4.78	$3.76e{-6}$	5.43
	80	$8.11e{-8}$	4.97	$1.33e{-7}$	4.82
	160	$2.58e{-9}$	4.97	$4.46e{-9}$	4.90
	320	$8.35e{-11}$	4.95	$1.45e{-10}$	4.94
ZSWENO	20	$7.38e{-5}$		$1.30e{-4}$	
	40	$2.53e{-6}$	4.87	$4.13e{-6}$	4.98
	80	$8.17e{-8}$	4.95	$1.41e{-7}$	4.88
	160	$2.64e{-9}$	4.95	$4.63e{-9}$	4.93
	320	$8.39e{-11}$	4.98	$1.40e{-10}$	5.04
MWENO	20	$1.86e{-5}$		$6.51e{-5}$	
	40	$3.85e{-7}$	5.59	$6.35e{-7}$	6.68
	80	$1.22e{-8}$	4.98	$2.03e{-8}$	4.97
	160	$3.83e{-10}$	4.99	$6.39e{-10}$	4.99
	320	$1.20e{-11}$	5.00	$2.00e{-11}$	5.00
ZWENO	20	$1.27e{-5}$		$3.44e{-5}$	
	40	$3.89e{-7}$	5.02	$6.55e{-7}$	5.71
	80	$1.22e{-8}$	4.99	$2.04e{-8}$	5.01
	160	$3.83e{-10}$	5.00	$6.40{-10}$	4.99
	320	$1.20e{-11}$	5.00	$2.00e{-11}$	5.00
U1WENO	20	$6.97e{-5}$		$1.72e{-4}$	
	40	$2.54e{-6}$	4.78	$3.79e{-6}$	5.50
	80	$8.11e{-8}$	4.97	$1.33e{-7}$	4.83
	160	$2.58e{-9}$	4.97	$4.46e{-9}$	4.90
	320	$8.35e{-11}$	4.95	$1.45e{-10}$	4.94
U1MWENO	20	$2.29e{-5}$		$7.24e{-5}$	
	40	$3.85e{-7}$	5.90	$6.35e{-7}$	6.83
	80	$1.22e{-8}$	4.98	$2.03e{-8}$	4.97
	160	$3.83e{-10}$	4.99	$6.39e{-10}$	4.99
	320	$1.20e{-11}$	5.00	$2.01e{-11}$	4.99
U1ZWENO	20	$1.34e{-5}$		$3.70e{-5}$	
	40	$3.89e{-7}$	5.11	$6.57e{-7}$	5.82
	80	$1.22e{-8}$	4.99	$2.04e{-8}$	5.01
	160	$3.83e{-10}$	4.99	$6.40e{-10}$	4.99
	320	$1.20e{-11}$	5.00	$2.00e{-11}$	5.00
UWWENO	20	$6.96e{-5}$		$1.61e{-4}$	
	40	$2.54e{-6}$	4.78	$3.76e{-6}$	5.42
	80	$8.11e{-8}$	4.97	$1.33e{-7}$	4.82
	160	$2.58e{-9}$	4.97	$4.46e{-9}$	4.90
	320	$8.35e{-11}$	4.95	$1.45e{-10}$	4.94

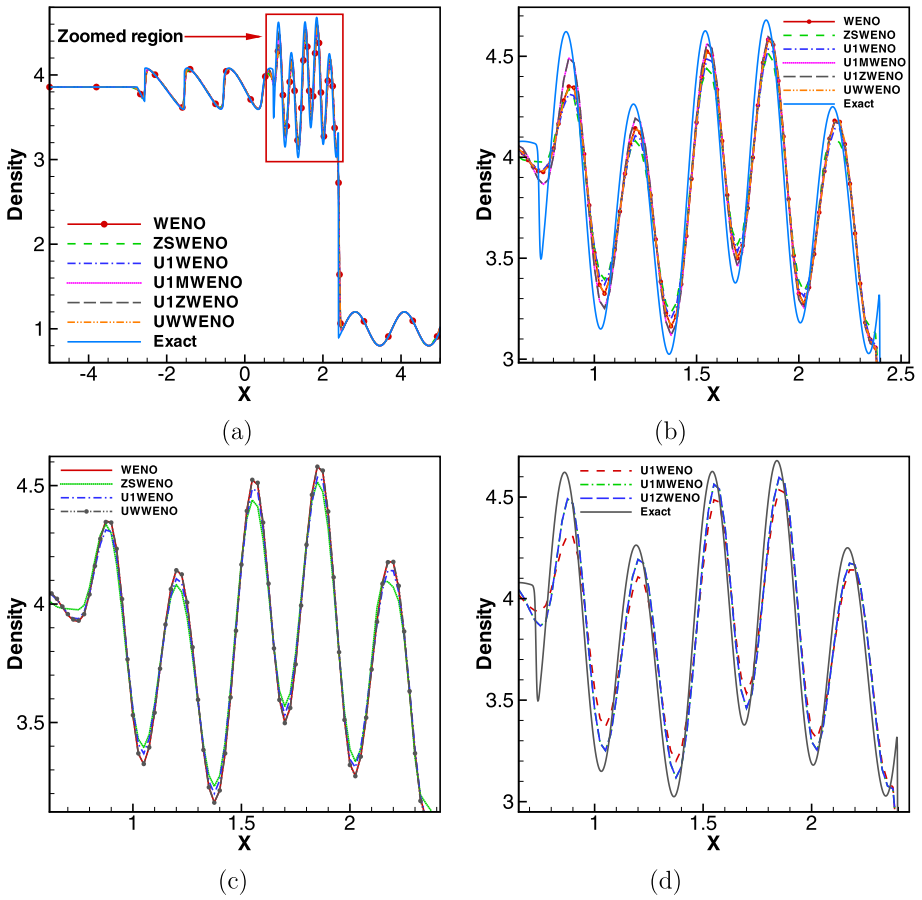

Fig. 12 Density distribution of the Shu-Osher problem by fifth order WENO schemes with 400 grid points at $t = 1.8$. The "exact" solution is obtained by the fifth order original WENO scheme with 8000 grid points. (**a**) Global view, (**b**) Zoomed view in the boxed region, (**c**) Comparison among WENO, ZSWENO, U1WENO and UWWENO, (**d**) Comparison among U1WENO, U1MWENO and U1ZWENO

Considering a balance between the convergence property, accuracy near smooth extrema and the CPU cost, we recommend the original fifth order WENO scheme in [8] combined with the first order upwind interpolation as the best method for steady state computation, and the improved WENO scheme in [2] combined with the first order upwind interpolation as the best method for the computation of multiscale problems.

6 Concluding Remarks

The convergence to steady state solutions of the Euler equations for WENO schemes with the Lax-Friedrichs flux splitting is studied through numerical experiments. The numerical experiments show that there is a slight post-shock oscillation which results in the residue hanging at a relatively high value instead of settling down to machine zero.

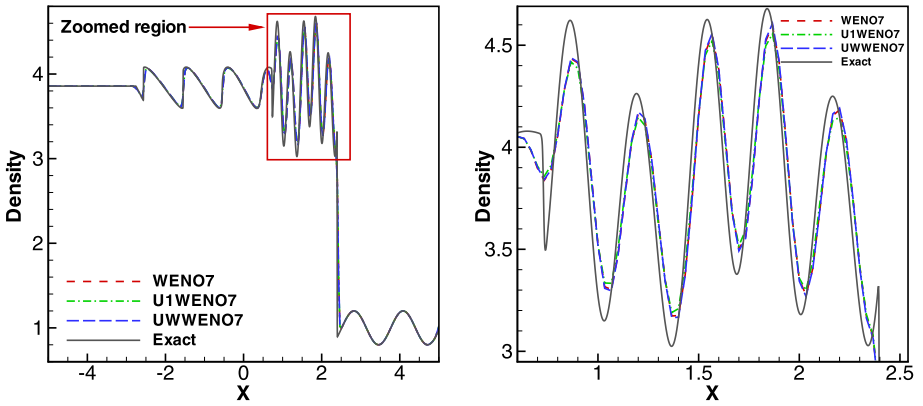

Fig. 13 Density distribution of Shu-Osher problem by the seventh order WENO schemes with 300 grid points at $t = 1.8$. The "exact" solution is obtained by the fifth order original WENO scheme with 8000 grid points. *Left*: Global view; *right*: Zoomed view in the boxed region

Through systemic numerical tests, we observe that there are many factors which may influence the appearance of the slight post-shock oscillation. The choice of the smoothness indicator and the local characteristic decomposition procedure are two examples.

In our earlier work [20], we proposed a new smoothness indicator that seems suitable for the simulation in the near region of shock waves. With this new smoothness indicator, the post-shock oscillation is removed or greatly reduced. The residue can settle down to machine zero for some cases and can be reduced significantly for other cases. However, this new smoothness indicator is difficult to be generalized to higher order WENO schemes, and it may lead to accuracy degeneracy near certain high order critical points.

In this paper, we use upwind-biased interpolation to approximate the physical variables including the velocity and enthalpy on the cell interface to compute the eigenvectors of the Jacobian used in the local characteristic decomposition. The upwind-biased interpolation contains the first order, the second order and the optimal order by the WENO technique. This process does not affect the high order accuracy of the WENO schemes. With this new technique, the slight post-shock oscillation can be removed for some problems and the residue can settle down to machine zero.

The convergence seems also to be influenced by the boundary condition and the angle between the grid line and shock waves for the flow that contains complex shock structure. This is a complicated issue and we have not been able to identify suitable boundary conditions when the shock passes through the boundary in order to reduce the WENO residue to machine zero. This issue is left for future study.

Acknowledgements Research of S. Zhang is supported by the Chinese National Natural Science Foundation grants 10572146, 10772193 and 973 program 2009CB724104. Research of C.-W. Shu is supported by AFOSR grant FA9550-09-1-0126 and NSF grant DMS-0809086.

References

1. Balsara, D.S., Shu, C.-W.: Monotonicity preserving weighted essentially non-oscillatory schemes with increasingly high order of accuracy. J. Comput. Phys. **160**, 405–452 (2000)
2. Borges, R., Carmona, M., Costa, B., Don, W.S.: An improved weighted essentially non-oscillatory scheme for hyperbolic conservation laws. J. Comput. Phys. **227**, 3191–3211 (2008)

3. Colonius, T., Lele, S.K.: Computational aeroacoustics: progress on nonlinear problems of sound generation. Prog. Aerosp. Sci. **40**, 345–416 (2004)
4. Donat, R., Marquina, A.: Capturing shock reflections: An improved flux formula. J. Comput. Phys. **125**, 42–58 (1996)
5. Harten, A.: High resolution schemes for hyperbolic conservation laws. J. Comput. Phys. **49**, 357–393 (1983)
6. Harten, A., Engquist, B., Osher, S., Chakravarthy, S.: Uniformly high order essentially non-oscillatory schemes, III. J. Comput. Phys. **71**, 231–303 (1987)
7. Henrick, A.K., Aslam, T.D., Powers, J.M.: Mapped weighted essentially non-oscillatory schemes: achieving optimal order near critical points. J. Comput. Phys. **207**, 542–567 (2005)
8. Jiang, G.-S., Shu, C.-W.: Efficient implementation of weighted ENO schemes. J. Comput. Phys. **126**, 202–228 (1996)
9. Liu, X.-D., Osher, S., Chan, T.: Weighted essentially non-oscillatory schemes. J. Comput. Phys. **115**, 200–212 (1994)
10. Liu, Y.-Y., Shu, C.-W., Zhang, M.: On the positivity of linear weights in WENO approximations. Acta Math. Appl. Sinica **25**, 503–538 (2009)
11. Roe, P.L.: Approximate Riemann solvers, parameter vectors, and difference schemes. J. Comput. Phys. **43**, 357–372 (1981)
12. Saad, M.A.: Compressible Fluid Flow. Prentice Hall, New York (1993)
13. Sebastian, K., Shu, C.-W.: Multi domain WENO finite difference method with interpolation at subdomain interfaces. J. Sci. Comput. **19**, 405–438 (2003)
14. Serna, S., Marquina, A.: Power ENO methods: a fifth-order accurate weighted power ENO method. J. Comput. Phys. **194**, 632–658 (2004)
15. Shu, C.-W.: High order weighted essentially non-oscillatory schemes for convection dominated problems. SIAM Rev. **51**, 82–126 (2009)
16. Shu, C.-W., Osher, S.: Efficient implementation of essentially non-oscillatory shock capturing schemes. J. Comput. Phys. **77**, 439–471 (1988)
17. Shu, C.-W., Osher, S.: Efficient implementation of essentially non- oscillatory shock capturing schemes II. J. Comput. Phys. **83**, 32–78 (1989)
18. Zhang, S., Zhang, Y.-T., Shu, C.-W.: Multistage interaction of a shock wave and a strong vortex. Phys. Fluid **17**, 116101 (2005)
19. Zhang, S., Zhang, H., Shu, C.-W.: Topological structure of shock induced vortex breakdown. J. Fluid Mech. **639**, 343–372 (2009)
20. Zhang, S., Shu, C.-W.: A new smoothness indicator for the WENO schemes and its effect on the convergence to steady state solution. J. Sci. Comput. **31**, 273–305 (2007)